Journal of Solid State Chemistry 184 (2011) 1273–1278

Contents lists available at ScienceDirect

Journal of Solid State Chemistry

journal homepage: www.elsevier.com/locate/jssc

Intrinsic ferromagnetic properties in Cr-doped ZnO diluted magnetic semiconductors

Yang Liu [a,b,c], Yanting Yang [a,b], Jinghai Yang [a,b,*], Qingfeng Guan [c,**], Huilian Liu [a,b], Lili Yang [a,b], Yongjun Zhang [a,b], Yaxin Wang [a,b], Maobin Wei [a,b], Xiaoyan Liu [a,b], Lianhua Fei [a,b], Xin Cheng [a,b]

[a] Institute of Condensed State Physics, Jilin Normal University, Siping 136000, People's Republic of China
[b] Key Laboratory of Functional Materials Physics and Chemistry of the Ministry of Education, Jilin Normal University, Siping 136000, Jilin, China
[c] School of Material Science and Engineering, Jiangsu University, Zhenjiang 210013, People's Republic of China

ARTICLE INFO

Article history:
Received 9 December 2010
Received in revised form
19 March 2011
Accepted 26 March 2011
Available online 2 April 2011

Keywords:
Semiconductors
Sol–gel method
XAFS
Magnetic properties

ABSTRACT

The Cr-doped zinc oxide ($Zn_{1-x}Cr_xO$, $0 \le x \le 0.08$) diluted magnetic semiconductors have been synthesized successfully by the sol–gel method. Investigations on magnetic, optical and structural properties of the produced samples have been done. Energy dispersive spectroscopy (EDS) shows the existence of Cr ion in the Cr-doped ZnO. The results of X-ray diffraction (XRD), the transmission electron microscope (TEM), X-ray photoelectron spectroscopy (XPS) and X-ray absorption fine structure (XAFS) indicate that the Cr ions are at least partially substitutionally incorporated into the crystal lattice of ZnO. The produced samples show good high-T_c (Curie temperature) ferromagnetism (FM) in Cr-doped ZnO nanoparticles with Cr concentration of less than 5 at%. The results of photoluminescence (PL) further testify that FM is an intrinsic property of the Cr-doped ZnO nanoparticles. And the occurrence of FM should mainly contribute to the Cr doping.

1. Introduction

Diluted magnetic semiconductors (DMSs) have been extensively studied because of the potential applications in the spintronic devices that allow the control of both the spin and the charge of the carriers [1,2]. Nowadays, extensive efforts have been made to study wide-band-gap oxide/nitride DMSs, such as the transition metal doped ZnO, TiO_2, SnO_2, In_2O_3 and GaN [3–5]. To realize the practical spintronic devices, it is essential that the DMS systems display FM at room temperature. In the quest for materials with a high transition temperature, transition metal (TM)-doped ZnO has emerged as an attractive candidate according to both theoretical and experimental studies. Stable ferromagnetic configurations arising from carrier-mediated exchange interactions have been predicted for several TM (Fe, Co, Ni and Cr)-doped ZnO DMSs [6,7]. The FM at room temperature has been observed in the experiment [8]. A drawback of this approach is that the dopant material can segregate to form precipitates or clusters that are actually responsible for the ferromagnetic properties. Hao et al. [9] and Li et al. [10]also pointed out the inhomogenous distribution of TM ions had important effects on the structure and magnetic properties of DMSs.

Among these dopant elements, trivalent Cr^{3+} ions exhibit $3d^3$ high-spin configuration, which may help to generate large magnetic moments in the host semiconductors [11]. In particular, Cr is an intrinsically nonmagnetic transition metal, its clusters or compounds (expect nanocrystalline CrO_2) do not contribute to FM. Therefore, to some extent, the study of the Cr-doped ZnO DMSs can effectively tell whether the FM originates from the existence of magnetic clustering or not.

Until now, most of the studies on the Cr-doped ZnO have focused on the thin film supported by the substrate [12–16]. The reproductive rate of the thin film is low, and the more important fact is that the lattice constant of the substrate does not usually match with that of ZnO, so that will cause the lattice distortion of ZnO [17]. This is adverse for studying the nature of the ZnO-based DMS thin film. Large variations in magnetic properties have been reported for otherwise similar films, indicating a strong dependence on synthesis and processing conditions [18–20]. Therefore, the problems as how to achieve the effective control of the preparation of materials, how to repeatedly prepare ZnO-based DMS nanomaterials with the crystal structure, good stability of the magnetic properties and especially FM at room temperature are of more concern. However, little knowledge about the preparation of free-standing ZnO-based DMS nanomaterials has ever been reported. So this study is necessary and urgent.

* Corresponding author at: Institute of Condensed State Physics, Jilin Normal University, Siping 136000, People's Republic of China. Fax: +86 434 3294566.
** Corresponding author. Tel.: +86 511 88790083; fax: +86 434 3294566.
E-mail addresses: jhyang1@jlnu.edu.cn (J. Yang), guanqf@ujs.edu.cn (Q. Guan).

0022-4596/$ - see front matter © 2011 Elsevier Inc. All rights reserved.
doi:10.1016/j.jssc.2011.03.049

Because of the convenient operation and the easy control, the sol–gel method has been extensively applied in the synthesis of the oxidate nanoparticles. In the present work, $Zn_{1-x}Cr_xO$ (x=0.00, 0.01, 0.02, 0.03, 0.04, 0.05, and 0.08) nanoparticles were synthesized by sol–gel method. We mainly study the behavior of the Cr-doping on PL property and FM in ZnO nanoparticles. The origin of FM in $Zn_{1-x}Cr_xO$ ($x \leq 0.05$) is also discussed.

2. Experimental details

2.1. Preparation of Cr-doped ZnO nanoparticles

Zinc nitrate hexahydrate [$Zn(NO_3)_2 \cdot 6H_2O$] and the appropriate amounts of chromium nitrate nonahydrate [$Cr(NO_3)_3 \cdot 9H_2O$] were dissolved into citric acid monohydrate ($C_6H_8O_7 \cdot H_2O$) with stirring to form the sol. Then, the mixture was polymerized to form the gel. We sintered the produced gel at 400 °C, and the Cr-doped ZnO nanoparticles were obtained.

2.2. Characterization techniques

Structure characterization of $Zn_{1-x}Cr_xO$ was performed by XRD on D/max-2500 copper rotating-anode X-ray diffractometer with Cu $K\alpha$ radiation (40 kV, 200 mA). The size distribution and the interplanar distance were investigated by TEM (200 keV, JEM-2100HR, Japan). XAFS measurements for the Cr K-edge were performed in the fluorescence mode at room temperature on the XAFS station of the U7C beam line of the National Synchrotron Radiation Laboratory (NSRL, Hefei, China). The magnetic hysteresis loops of $Zn_{1-x}Cr_xO$ were measured by a Lake Shore 7407 vibrating sample magnetometer (VSM). The valence state of the Cr element was analyzed by XPS (VG ESCALAB Mark II). PL measurement was performed on an HR800 Labram Infinity Spectrophotometer, excited by a continuous He–Cd laser at a wavelength of 325 nm and a power of 50 mW.

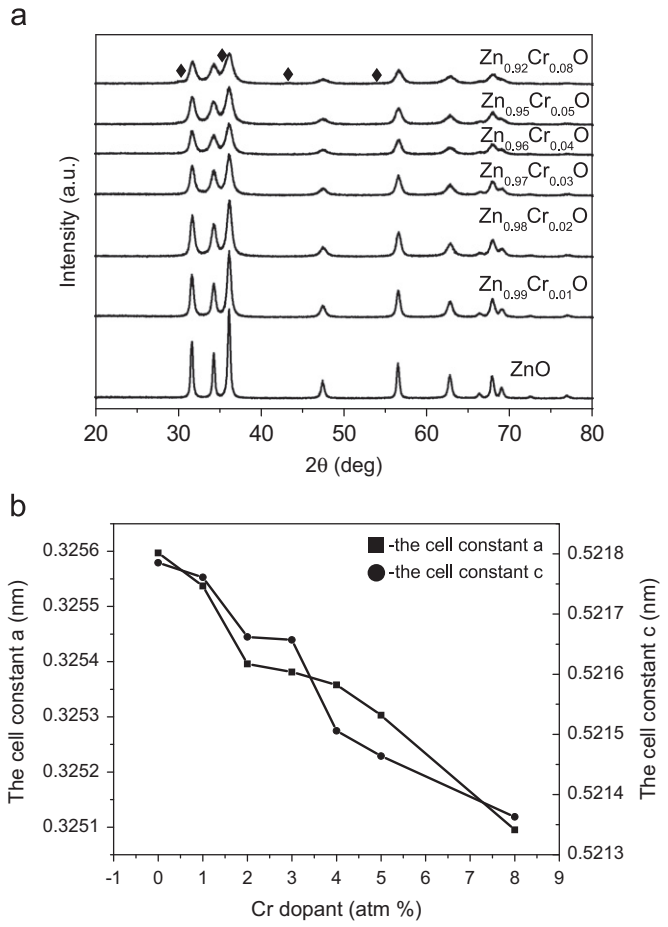

Fig. 1. XRD patterns of the undoped ZnO and the Cr-doped ZnO (a); the change in the cell constants a and c of ZnO with different Cr concentrations (b). "♦" indicates the peaks of the impurity phase of $ZnCr_2O_4$.

3. Results and discussion

3.1. Structural characterization

Fig. 1(a) shows the XRD patterns of the undoped ZnO and $Zn_{1-x}Cr_xO$ (x=0.01, 0.02, 0.03, 0.04, 0.05, and 0.08). All diffraction peaks can be indexed to wurtzite the hexagonal ZnO (space group $P63mc$) with Cr concentration of less than 5 at%. In addition, no hints of the Cr metal or the Cr oxides are found. The secondary phase of $ZnCr_2O_4$ emerges at x=0.08, which indicates that the doping limit for Cr in ZnO here is below 8%. As for the undoped ZnO, the cell constant is estimated to be a=0.3256 nm and c=0.5218 nm. While, as for the Cr-doped ZnO, with the increase of the Cr content, the cell constant decreases. Fig. 1(b) exhibits the dependence of the Cr content on the lattice constants a and c of the $Zn_{1-x}Cr_xO$ nanoparticles. Such a rapid lattice contraction can be qualitatively understood in terms of the sizes of the ions and their local coordinations. To sum up, this result may originate from the substitutions of Cr ions with a small ionic radius of 0.063 nm for the Zn (0.074 nm) sites [21]. That justifies the considerable lattice contraction. Moreover, we find that the width of the X-ray peak increases. With the increase of the Cr concentration, the phenomenon becomes more obvious. It suggests a decrease of the mean particle sizes in the crystalline correlation. The mean particle size of $Zn_{1-x}Cr_xO$ (x=0.00, 0.01, 0.02, 0.03, 0.04, 0.05, and 0.08) is 26.2, 16.9, 13.4, 11.1, 10.1, 9.8 and 8.1 nm by Debye–Scherrer formula, respectively. Many theoretical and experimental studies have demonstrated size-dependent lattice contraction [22,23]. So the size effect should be the other possible reason of the lattice contraction due to the variation of the surface stresses. The reason why the Cr-doping restrains the growth of the crystal lattice is also analyzed in the previous work [24].

The morphology and structure were characterized by TEM and HRTEM (high-resolution TEM). The images of $Zn_{1-x}Cr_xO$ (x=0.03, 0.05 and 0.08) samples (a)–(f) are shown in Fig. 2. The average particle size is about 11, 10 and 8 nm for $Zn_{1-x}Cr_xO$ (x=0.03, 0.05 and 0.08), respectively, which are in agreement with the results of XRD. In addition, it can be clearly observed that the interplanar distance of the fringes is 0.26 nm, matching the (0 0 2) planes of the wurtzite ZnO from the HRTEM figures of all $Zn_{1-x}Cr_xO$ samples. The interplanar distance of the fringes is 0.25 nm from the HRTEM figures of the $Zn_{0.92}Cr_{0.08}O$, which is corresponding to the (3 1 1) planes of $ZnCr_2O_4$. Moreover, the inset of Fig. 2(b), (d), and (f) is the EDS spectrum of a single Cr-doped ZnO nanoparticle. EDS shows the existence of the Cr ion in the Cr-doped ZnO. The content of Cr is about 2.6%, 4.8% and 7.2%, respectively, which is consistent with the design of our experiment. These results further testify the probability that Cr ions have been substitutionally incorporated into the crystal lattice of ZnO.

3.2. Chemical characterization

The XPS results of the $Zn_{1-x}Cr_xO$ (x=0.03, 0) nanoparticles annealed at 400 °C are shown in Fig. 3. As for the $Zn_{0.97}Cr_{0.03}O$ (Fig. 3(a)), the XPS spectrum shows that the indexed peaks are corresponding to those of C, Cr, O and Zn. Among them, because

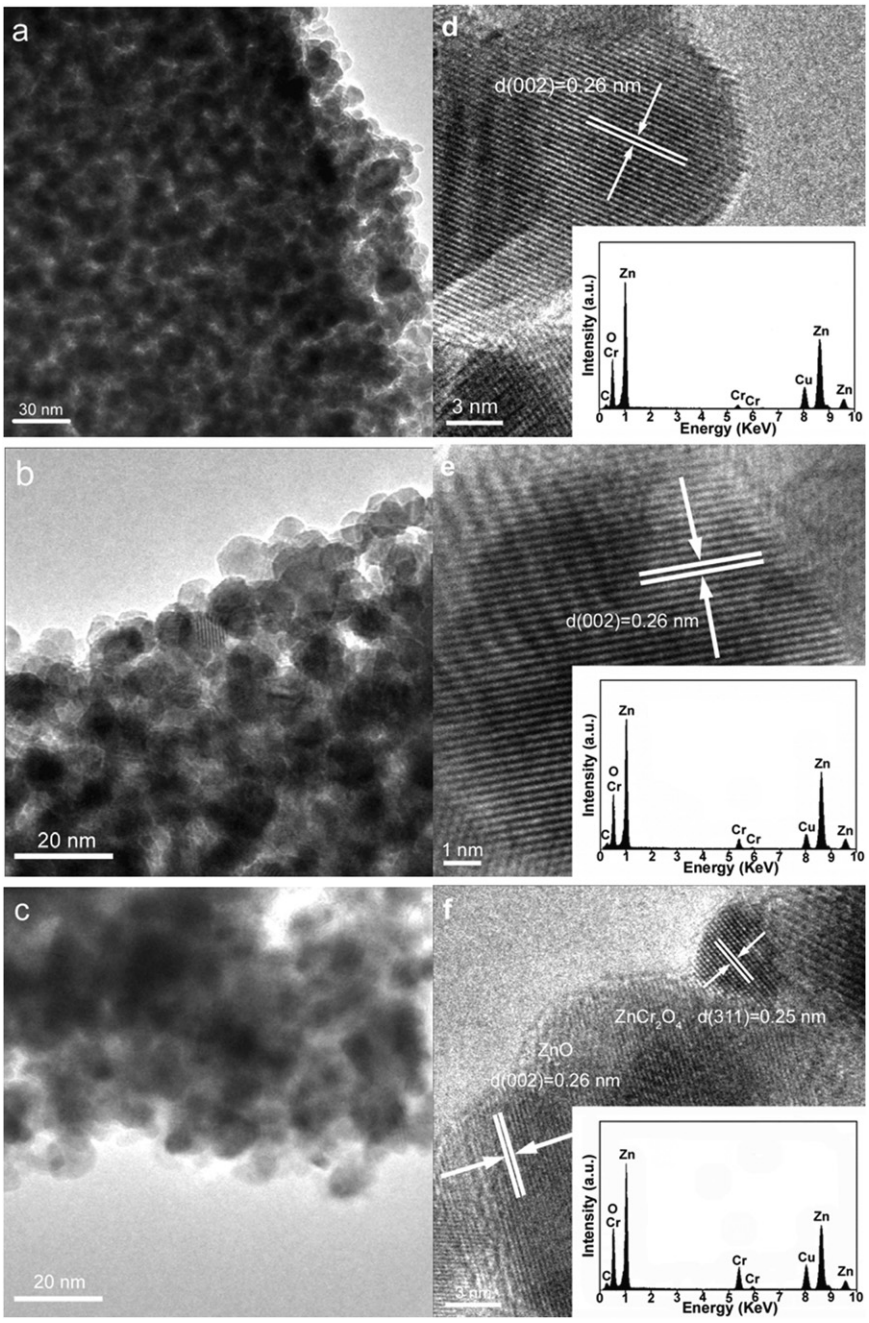

Fig. 2. TEM and HRTEM images of the Cr-doped ZnO nanoparticles. (a), (b) and (c) is the TEM image of $Zn_{1-x}Cr_xO$ ($x=0.03$, 0.05, and 0.08) nanoparticles; (d), (e) and (f) is the HRTEM image of $Zn_{1-x}Cr_xO$ ($x=0.03$, 0.05, and 0.08) nanoparticles, respectively. The inset figure is the EDS spectrum.

the citrate is not completely decomposed, carbon arises during the process of sintering the precursors. The survey scans show no magnetic impurity within the detection limit. The high resolution scans of the XPS spectra of Cr 2*p* have been shown in the inset of Fig. 3(a). Based on the Gauss fitting, the peaks of Cr $2p_{3/2}$ are detected at 576.6 eV for the sample. The positions of the peaks are different from those of 574.2 eV of Cr metal, 579.0 eV of Cr^{6+} and 576.0 eV of Cr^{2+}, but it is very close to the peak position of Cr $2p_{3/2}$ (576.7 eV) in Cr_2O_3 [8]. It suggests that the Cr dopants are incorporated into the ZnO lattice as Cr^{3+} ions. Moreover, the intensity of the Cr $2p_{1/2}$ is stronger than that of Cr $2p_{3/2}$. The main reason is that the overlap of the XPS photoelectron of Cr $2p_{1/2}$ located at 585.2 eV and the Auger electron peak of Zn located at 585 eV leads to the phenomenon [25]. The inset of Fig. 3(b) shows the valence bonds of Zn $2p_{3/2}$ states of the $Zn_{1-x}Cr_xO$ ($x=0.03$, 0) nanoparticles. The positions of Zn $2p_{3/2}$ peaks slightly shift towards the higher binding energy side, with the increase of Cr concentration from 0% to 3%, owing to the change in the chemical environment resulting from the incorporation of Cr in ZnO nanoparticles. The result further testifies the probability that the Cr^{3+} ions take the place of Zn^{2+} sites. The similar phenomena were reported by Lee et al. [26].

3.3. XAFS study

XAFS analysis, i.e., extended X-ray absorption fine structure (EXAFS) and X-ray absorption near-edge spectroscopy (XANES), is usually one recognized practical way to study the arrangement of atoms in materials without long range order. In XAFS, the number and species of neighbor atoms, their distance from the selected

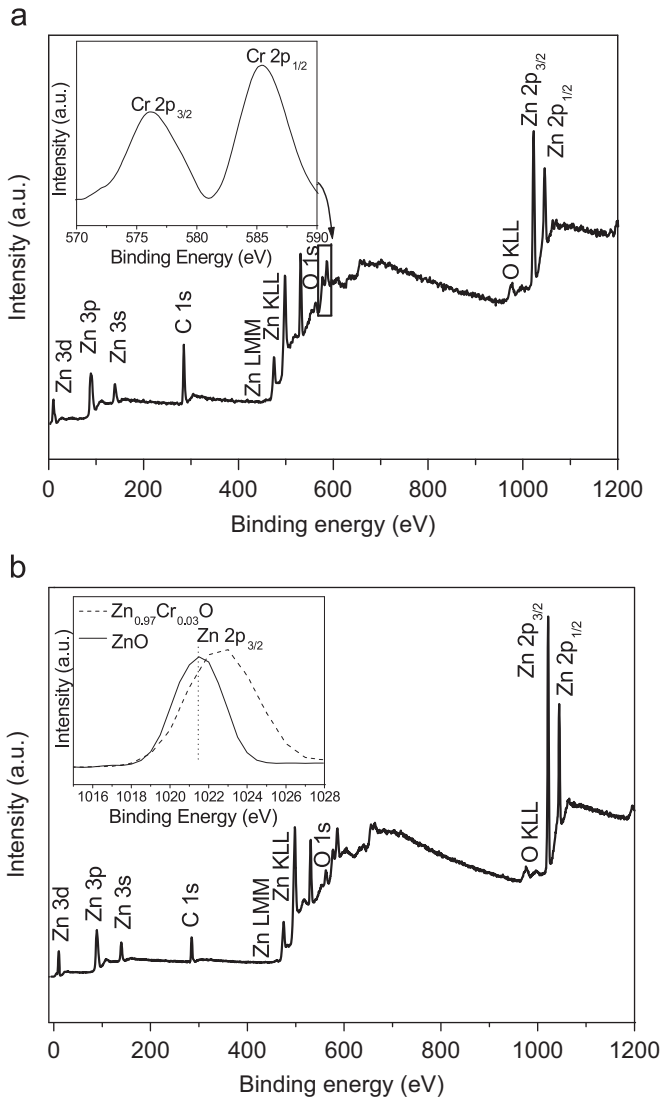

Fig. 3. XPS spectrum of the $Zn_{1-x}Cr_xO$ ($x=0.03$, 0) nanoparticles. The inset is the detail scans of Cr $2p_{3/2}$ and $2p_{1/2}$ peaks (a); the inset is the detail scans of Zn $2p_{3/2}$ peaks of the $Zn_{1-x}Cr_xO$ ($x=0.03$, 0) nanoparticles (b).

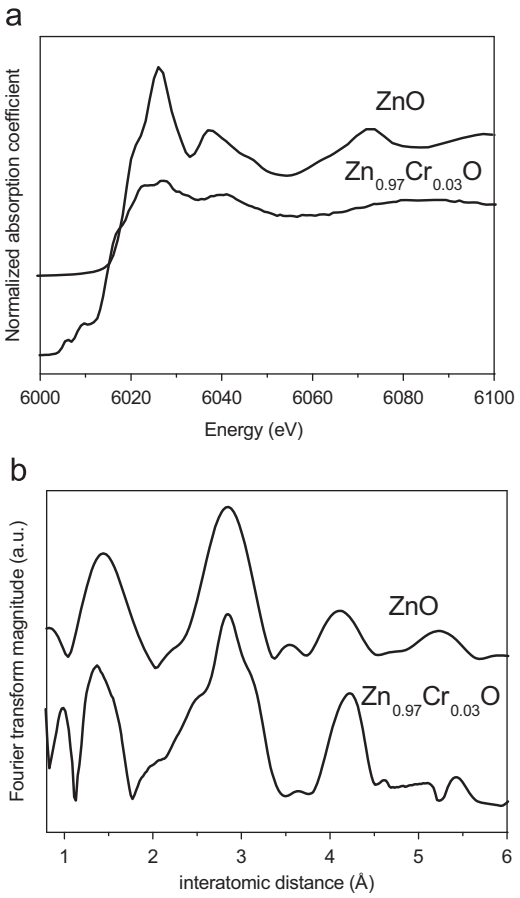

Fig. 4. (a) Zn K-edge XANES spectra of the undoped ZnO and Cr K-edge XANES spectra of the $Zn_{0.97}Cr_{0.03}O$. The Zn K-edge XANES spectra is moved to the position of Cr K-edge XANES spectra of the $Zn_{0.97}Cr_{0.03}O$. (b) The Fourier transform magnitude of the undoped ZnO and the $Zn_{0.97}Cr_{0.03}O$.

atom and the thermal or structural disorder of their positions can be determined from the oscillatory part of the absorption coefficient above a major absorption edge. Fig. 4(a) shows the Cr K-edge XANES spectra of the $Zn_{0.97}Cr_{0.03}O$ and the Zn K-edge XANES spectra of the undoped ZnO. In order to compare above-mentioned two samples conveniently, we move the Zn K-edge XANES spectra to the position of Cr K-edge XANES spectra parallelly. The Cr K-edge features of the $Zn_{0.97}Cr_{0.03}O$ and Zn K-edge features of the undoped ZnO are similar, showing that the chemical environment of Cr in the $Zn_{0.97}Cr_{0.03}O$ is the same as that of Zn in the undoped ZnO. So we believe that the Cr ions have dissolved into ZnO lattice and the substituted Zn ions at least partially. In addition, the XANES spectra of the $Zn_{0.97}Cr_{0.03}O$ and the Cr_2O_3 are almost the same [11], which indicate that the valence state of Cr in the $Zn_{0.97}Cr_{0.03}O$ is $+3$. It is consistent with the results of the XPS, which further testifies the probability that the Cr ions take the place of Zn sites in our samples. However, the XANES curve of the $Zn_{0.97}Cr_{0.03}O$ is obviously different from those of Cr metal and other chromium oxides [27,28], indicating no Cr metal or Cr-related compounds are formed in our samples.

Fig. 4(b) compares the Fourier transform amplitude of the undoped ZnO, as is obtained from the Zn K-edge EXAFS data, with that of the $Zn_{0.97}Cr_{0.03}O$ from the Cr K-edge spectrum. The first and the second major peaks in the radial distribution functions of the undoped ZnO correspond to the nearest oxygen and Zn from the central Zn atoms, respectively [29]. For the $Zn_{0.97}Cr_{0.03}O$, the two strong peaks correspond to the nearest oxygen and Zn (Cr) from the central Cr atoms. This figure indicates that the results of the radial distribution functions of the undoped ZnO and the $Zn_{0.97}Cr_{0.03}O$ are very similar. The inter-atomic distances between the two major peaks of the undoped ZnO are essentially the same as those of the $Zn_{0.97}Cr_{0.03}O$. So the Cr ions in the $Zn_{0.97}Cr_{0.03}O$ shows a similar radial structure to Zn ions in the undoped ZnO.

3.4. Magnetic properties

Magnetic measurements on $Zn_{1-x}Cr_xO$ ($x=0.01$, 0.02, 0.03, 0.04, 0.05, and 0.08) were performed at room temperature, using vibrating sample magnetometer. Fig. 5 shows the magnetization versus magnetic field (M–H) loops. The inset of Fig. 5 shows the M–H loop of undoped ZnO. The result shows the undoped ZnO is paramagnetic at room temperature. However, the 3 at% doped sample shows clear magnetic hysteresis loops. That indicates good high-T_c FM in Cr-doped ZnO nanoparticles. Similar results are found in other Cr concentration of less than 5 at%. The $Zn_{0.97}Cr_{0.03}O$ individual possesses moment of 0.004 μ_B per Cr atom. This result has a good agreement with the value in Ref. [30]. But it is much less than the theoretically calculated value (3.7 μ_B) [31]. On one hand, the weaker change between particles in the nanostructural materials can lower the magnetic moment due to the nanostructural nature of the material. On the other

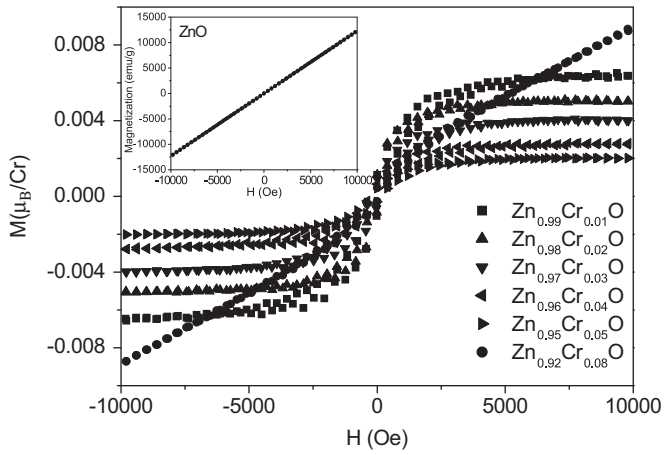

Fig. 5. Magnetic hysteresis (M–H) loops of $Zn_{1-x}Cr_xO$ (x=0.01, 0.02, 0.03, 0.04, 0.05, and 0.08) at room temperature under 10 KOe. The inset shows the M–H loop of undoped ZnO.

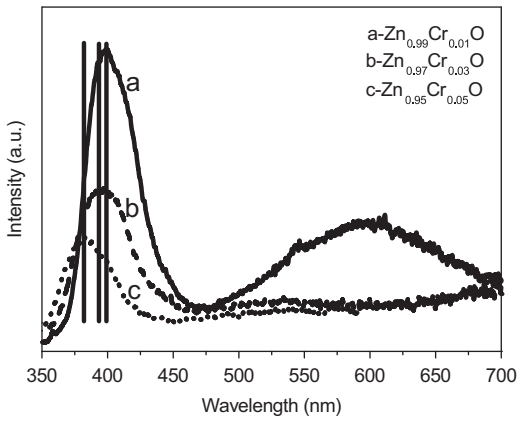

Fig. 6. PL spectra of $Zn_{1-x}Cr_xO$ nanoparticles (x=0.01, 0.03, and 0.05).

hand, once the concentration of Cr is very close to the cationic percolation threshold, nearest-neighbor antiferromagnetic interation between the Cr ions can lower the magnetic moment. Both antiferromagnetism and ferromagnetism exist in the Cr ions. Owing to the competition with antiferromagnetism, ferromagnetic behavior is limited.

In addition, with the increase of the Cr concentration, the magnetic comment per Cr atom decreases. The 1% Cr sample possessed a net moment of 0.006 μ_B/Cr, and the 5% Cr sample has a moment of 0.002 μ_B/Cr. The variation tendency has a good agreement with that in Ref. [12]. The consistent drop in magnetic moment might be resulted by the increase of the antiferromagnetic coupling occurring at the shorter distances between Cr pairs [32]. It is worth to note that, $Zn_{0.92}Cr_{0.08}O$ nanoparticles are not saturated in the field of 10,000 Oe. That indicates that they are the mixtures of the ferromagnetic materials and the paramagnetic materials. According to the results of XRD, we think that $ZnCr_2O_4$ in the sample contributes to this phenomenon. $ZnCr_2O_4$ itself has antiferromagnetic properties, and its neel temperature (T_n) is 11 K [33]. Similarly, if other samples contain $ZnCr_2O_4$, they should show the same results. However, the result of the measurement shows the FM, which can be used to identify the fact that other samples have no $ZnCr_2O_4$ phase. It is known that the secondary phases are a concern in any diluted magnetic system as a source of the spurious magnetic signal. Neither CrO_2 nor other phases (antiferromagnetic Cr metal, Cr_2O_3 and Cr_3O_4) are detected via XRD. Indeed, the sensitivity of XRD may not be the best to identify the minute amounts of second phases in the samples. It is fortunate that these phases (Cr metal, Cr_2O_3 and Cr_3O_4) can be present in small quantities, FM should not be related to these phases because their Neel temperature are below the room temperature. The stronger ferromagnetic behavior in samples with lower concentrations of Cr and its apparent weakening and subsequent disappearance at higher doping concentrations also confirm the absence of the ferromagnetic CrO_2. In addition, CrO_2 is metastable, it is unlikely to form under the low oxygen pressure conditions usually employed in vaccum deposition technique [34]. As is discussed above, the observed FM is not from the secondary phases. We conclude that FM of the $Zn_{1-x}Cr_xO$ in this study is an intrinsic property of the Cr-doped ZnO.

3.5. Optical properties

Fig. 6 shows PL spectra of the $Zn_{1-x}Cr_xO$ nanoparticles (x=0.01, 0.03, and 0.05) at room temperature. The PL spectra of all the $Zn_{1-x}Cr_xO$ nanoparticles contain a strong ultraviolet (UV) emission peak. The UV emission originates from the excitonic recombination, which is corresponding to the near-band-edge (NBE) [35,36]. It can be seen from Fig. 6 that the UV emission peak position of the Cr-doped ZnO nanoparticle exhibits blue shift with the increase of Cr concentration. The UV emission band is sharply suppressed as well. This indicates that the Cr doping prompts the nonradiative recombination process and that the existence of the transition metal ions like Cr can control the excitonic recombination radiation. In addition, with the increase of the Cr concentration, the visible light (VL) emission band is also suppressed. Various mechanisms have been proposed for the VL emission of $Zn_{1-x}Cr_xO$. It is mainly related to the defects or the oxygen vacancies in ZnO [37,38]. Recently, Xing et al. even found the FM in undoped ZnO [39]. We assume that a specific defect is the main contribution to the FM. Based on the above assumptions, the related PL intensity of the VL emission should have the same decreasing trend with the increase of the Cr concentration as the magnetic moment of the $Zn_{1-x}Cr_xO$ nanoparticles. In Fig. 6, the relative PL intensities of the VL emission decrease steadily with the increase of the Cr concentration, which resembles the decreasing trend of the magnetic moment. In other words, to some extent, the defects may play an important role in the ferromagnetic origin of the $Zn_{1-x}Cr_xO$ nanoparticles [38]. However, the Cr doping restrains the appearance of the defects in ZnO. That might be another reason that the magnetic moment decreases with the increase of the Cr concentration. Therefore, it can be concluded that the observed FM is an intrinsic property of the Cr-doped ZnO nanoparticles. That is to say the FM should mainly contribute to the Cr doping.

4. Conclusions

In this paper, the Cr-doped zinc oxide ($Zn_{1-x}Cr_xO$) (x=0.00, 0.01, 0.02, 0.03, 0.04, 0.05, and 0.08) nanoparticles were successfully synthesized by sol–gel method. The results indicate that Cr ions have probably substituted for Zn ions successfully. The doped sample shows good high-T_c FM in the Cr^{3+} doped ZnO nanocrystals with the Cr concentration of less than 5 at%. However, in this concentration range, the magnetic moment decreases with the increase of the Cr concentration. The results of PL further testify that FM is an intrinsic property of the Cr-doped ZnO nanoparticles and FM should contribute mainly to the Cr doping. The results in our work provide an optimized concentration range of Cr^{3+} in ZnO to obtain both good optical and magnetic properties of the ZnO nanoparticles.

Acknowledgment

This work is supported by the National Programs for High Technology Research and Development of China (863) (Item no. 2009AA03Z303), the National Natural Science Foundation of China (Grant nos. 60878039), the National Youth Program Foundation of China (Grant nos. 10804036 and 10904050), Program for the development of Science and Technology of Jilin province (Item no. 20080514) and the Eleventh Five-Year Program for Science and Technology of Education Department of Jilin Province (Item no. 20090426).

References

[1] H. Ohno, Science 281 (1998) 951.
[2] S.A. Wolf, D.D. Awschalom, R.A. Buhrman, J.M. Daughton, S. von Molnar, M.L. Roukes, A.Y. Chtchelkanova, D.M. Treger, Science 294 (2001) 1488.
[3] X.Y. Xu, C.B. Cao, J. Alloys Compd. 501 (2010) 265.
[4] Mukta V. Limaye, Shashi B. Singh, Raja Das, Pankaj Poddar, Sulabha K. Kulkarni, J. Solid State Chem. 184 (2011) 391.
[5] G.Z. Xing, J.B. Yi, D.D. Wang, L. Liao, T. Yu, Z.X. Shen, C.H.A. Huan, T.C. Sum, J. Ding, T. Wu, Phys. Rev. B. 79 (2009) 174406.
[6] M. Peiteado, A.C. Caballero, D. Makovec, J. Solid State Chem. 180 (2007) 2459.
[7] M. Peiteado, D. Makovec, M. Villegas, A.C. Caballero, J. Solid State Chem. 181 (2008) 2456.
[8] B.Q. Wang, J. Iqbal, X.D. Shan, G.W. Huang, H.G. Fu, R.H. Yu, D.P. Yu, Mater. Chem. Phys. 113 (2009) 103.
[9] W.C. Hao, J.J. Li, H.Z. Xu, J.O. Wang, T.M. Wang, ACS Appl. Mater. Interfaces 2 (2010) 2053.
[10] J.J. Li, W.C. Hao, H.Z. Xu, T.M. Wang, J. Appl. Phys. 105 (2009) 053907.
[11] L. Schneider, S.V. Zaitsev, W. Jin, A. Kompch, M. Winterer, M. Acet, G. Bacher, Nanotechnology 20 (2009) 135604.
[12] L.J. Zhuge, X.M. Wu, Z.F. Wu, X.M. Chen, Y.D. Meng, Scri. Mater. 60 (2009) 214.
[13] J. Elanchezhiyan, K.P. Bhuvana, N. Gopalakrishnan, Yong Chang, S. Sivananthan, M. Senthil Kumar, T. Balasubramanian, J. Alloys Compd. 468 (2009) 7.
[14] Z.L. Lu, W. Miao, W.Q. Zou, M.X. Xu, F.M. Zhang, J. Alloys Compd. 494 (2009) 392.
[15] N. Al-Hardan, M.J. Abdullah, A. Abdul Aziz, H. Ahmad, Appl. Surf. Sci. 256 (2010) 3468.
[16] Y.M. Hu, C.W. Hsu, C.Y. Wang, S.S. Lee, J.W. Chiou, T.C. Han, G.J. Chen, W.Y. Chou, J. Chang, Thin Solid Films 518 (2010) 2916.
[17] S. Duhalde, M.F. Vignolo, F. Golmar, C. Chiliotte, M. Weissmann, Phys. Rev. B. 72 (2005) 161313.
[18] J. Elanchezhiyan, K.P. Bhuvana, N. Gopalakrishnan, B.C. Shin, W.J. Lee, T. Balasubramanian, J. Alloys Compd. 478 (2009) 45.
[19] Richa Bhargava, Prashant K. Sharma, Sanjeev Kumar, Avinash C. Pandey, Naresh Kumar, J. Solid State Chem. 183 (2010) 1400.
[20] Y.B. Li, Y. Li, M.Y. Zhu, T. Yang, J. Huang, H.M. Jin, Y.M. Hu, Solid State Commun. 150 (2010) 751.
[21] Y.M. Hu, Y.T. Chen, Z.X. Zhong, C.C. Yu, G.J. Chen, P.Z. Huang, W.Y. Chou, J. Chang, C.R. Wang, Appl. Surf. Sci. 254 (2008) 3873.
[22] C. Solliard, M. Flueli, Surf. Sci. 156 (1985) 487.
[23] H.S. Shin, J. Yu, J.Y. Song, H.M. Park, Appl. Phys. Lett. 94 (2009) 011906.
[24] Y. Liu, J.H. Yang, Q.F. Guan, L.L. Yang, Y.J. Zhang, Y.X. Wang, B. Feng, J. Cao, X.Y. Liu, Y.T. Yang, M.B. Wei, J. Alloys Compd. 486 (2009) 835.
[25] P. Prathap, N. Revathi, Y.P. Venkata Subbaiah, K.T. Ramakrishna Reddy, J. Phys.: Condens. Matter 20 (2008) 035205.
[26] S. Lee, D.Y. Kim, Y. Shon, C.S. Yoon, Appl. Phys. Lett. 89 (2006) 022120.
[27] J.A. Bearden, A.F. Burr, Rev. Mod. Phys. 39 (1967) 125.
[28] I. Arčon, B. Mirtič, A. Kodre., J. Am. Ceram. Soc. 81 (1998) 222.
[29] T.F. Shi, S.Y. Zhu, Z.H. Sun, S.Q. Wei, W.H. Liu, Appl. Phys. Lett. 90 (2007) 102108-1-3.
[30] D.W. Chu, Y.P. Zeng, D.L. Jiang, Solid State Commun. 143 (2007) 308.
[31] L.Y. Li, H. Li, X.G. Luo, X. Zhang, W.H. Wang, Y. Cheng, Q.G. Song, Solid State Commun. 146 (2008) 420.
[32] Q. Wang, Q. Sun, P. Jena, Y. Kawazoe, Appl. Phys. Lett. 87 (2005) 162509.
[33] S.H. Lee, C. Broholm, T.H. Kim, W. Ratcliff, S.W. Cheong, Phys. Rev. Lett. 84 (2000) 3718.
[34] Q. Zhao, J.J. Yuan, G.H. Wen, G.T. Zou, J. Magn. Magn. Mater. 320 (2008) 2356.
[35] D.D. Wang, G.Z. Xing, H.Y. Peng, T. Wu, J. Phys. Chem. C. 113 (2009) 7065.
[36] D.D. Wang, J.H. Yang, G.Z. Xing, L.L. Yang, J.H. Lang, M. Gao, B. Yao, T. Wu, J. Lumin. 129 (2009) 996.
[37] K. Sato, H. Katayama-Yoshida, Physica B. 308 (2001) 904.
[38] H. Liu, X. Zhang, L. Li, Y.X. Wang, K.H. Gao, Z.Q. Li, R.K. Zheng, S.P. Ringer, B. Zhang, X.X. Zhang, Appl. Phys. Lett. 91 (2007) 072511.
[39] G.Z. Xing, D.D. Wang, J.B. Yi, L.L. Yang, M. Gao, M. He, J.H. Yang, J. Ding, T.C. Sum, T. Wu, Appl. Phys. Lett. 96 (2010) 112511.